7th International Conference on Debris-Flow Hazards Mitigation

Deciphering debris-flow seismograms at Illgraben, Switzerland

Michaela Wenner[a,b,*], Fabian Walter[a], Brian McArdell[b], Daniel Farinotti[a,b]

[a]*Laboratory of Hydraulics, Hydrology and Glaciology (VAW), ETH Zurich, Hönggerbergring 26, 8093 Zürich, Switzerland*
[b]*Swiss Federal Insitute for Forest, Snow and Landscape Research (WSL), Zürcherstrasse 111, 8903 Zürich, Switzerland*

Abstract

Mass wasting, such as rockfalls, landslides and debris flows in steep mountain terrain, has a high destructive potential, and plays a key role in both erosion and landscape evolution. As an alternative to many conventional approaches, seismology allows monitoring of such mass movements at safe distances, provides estimates of event location and timing, and can give insights into dynamics and rheology granular flows. Here, we analyze seismic data recorded during the 2017 and 2018 debris-flow seasons at Illgraben, a steep canyon located in Switzerland. Yearly precipitation is controlled by summer rainstorms with high rainfall intensity during which mass wasting including rock-slope failure and debris flows occur regularly. The frequent debris-flow occurrence (on average three events per year) makes the Illgraben an ideal site for cross-validating a seismically-derived event catalog of mass movements with "ground-truth data", such as digital terrain models, flow depths estimates and other in-torrent measurements. We present seismic frequency characteristics of the Illgraben debris-flow series and investigate how the seismic signature depends on actual debris-flow characteristics, such as grain sizes, and on propagation effects of the generated seismic waves. Whereas these two effects are usually difficult to separate, the source component contains valuable information on the flow's material composition. Stations that are close to the torrent, we find that dominant frequencies in the recorded signal reflect the distance to the dominant source. For one particular station, this is shown on recordings of several events, where a dominant frequency of about 5.5 Hz indicates the passing of the flow at a 48m check dam. Power spectral densities at that instance give an estimate of the particle content of the debris flow. We also find that a jump in dominant frequency does not necessarily reflect the location of the flow front. Seismic studies of debris-flow dynamics and material composition should therefore not be limited to entire debris-flow seismograms, but instead focus on individual time windows and consider different sensors separately. The presented analysis underlines the use of seismic data in torrent and landscape studies.

Keywords: seismology, spectral chracteristics, monitoring, debris flow

1. Introduction

In mountainous areas, mass movements such as debris flows are a significant threat to infrastructure, properties and human life. Monitoring of debris-flow prone catchments is essential to improve our understanding of debris-flow dynamics, and needed for both designing mitigation measures and damage reduction. Standard granular flow models for debris flows assume a shallow propagating mass, in which the rheology is described by an effective friction (Mangeney-Castelnau et al., 2005; Mangeney et al., 2007; Christen et al., 2010). Field measurements are essential to constrain this effective friction and other parameters, including erosion, flow depth and flow density. Classical monitoring techniques, like radar altimeters, aerial imagery and geophones within the torrent, can give information about onset time, flow depth, discharge and erosion or deposition areas. However, they offer no direct measurements of flow characteristics such as effective friction and material density (for an overview in debris-flow monitoring instrumentation see Arattano & Marchi, 2008).

In recent years, seismology has evolved into a standard tool to study mass movements and their dynamics at high temporal resolution (Larose et al., 2015; Allstadt et al., 2018). Seismic signals generated by such events are often classified into low and high frequency content. The low frequency signal (< 10 s) is modelled by the elastic response

* Corresponding author e-mail address*: wenner@vaw.baug.ethz.ch*

the earth to acceleration and deceleration of the bulk mass of the flow (e.g. Ekström & Stark, 2013). In contrast, higher frequency signals (> 1 Hz) are generated by collisions of grains within the flow, and their impacts on the bed. For smaller scale mass movements, the force that is exerted on the earth is often too small to generate detectable low-frequency elastic waves. In contrast, high frequency signals can be recorded in such cases, and are used to study rockfalls and rock avalanches in both volcanic (e.g. Norris, 1994; Hibert et al., 2011; Hibert et al., 2017) and mountainous areas (eg. Deparis et al., 2008 ; Vilajosana et al., 2008; Dammeier et al., 2011; Burtin et al., 2014; Dietze et al., 2017; Provost et al., 2017) or snow avalanches (eg. Suriñach et al., 2005, Heck et al., 2018). Such signals are typically emergent with dominant frequencies of 5–10 Hz and no distinguishable seismic phases. Signal durations vary between seconds to several tens of seconds, depending on the type of movement. Consisting of numerous and overlapping individual particle-bed and inter-particle collisions, source models of the high frequency mass movement signals are far more complicated than the low frequency component of the signal, and are hence less understood.

Recently, Kean et al. (2015) and Lai et al. (2018) adapted a model of fluvial bedload transport to explain the high-frequency seismic spectrum of debris flows in sediment-filled channels, and during a debris flow in California, respectively. The model explains the seismic signal in terms of instantaneous Hertzian impacts of bedload particles on the ground. In this way, the impact force generating seismic waves results from a change in the particles' linear momentum (impulse), which is two times the product of the particle's initial mass and velocity (Tsai et al., 2012). To simplify the model for debris flows, these impacts are integrated over the boulder-rich flow front.

The adapted Tsai et al. (2012) model makes assumptions for particle velocities and seismic path effects describing the propagation of seismic waves from the river bed to a recording unit. Importantly, the calculated seismic spectrum is influenced by the poorly constrained grain size distributions of moving particles, as well as seismic velocities and attenuation of ground substrate influence. Nevertheless, the model explains observed seismic frequency spectra for bedload transport (Burtin et al., 2008). For debris flows, the model proposes that spectral amplitudes are primarily influenced by the grain sizes of the boulder-rich debris-flow front. Furthermore, the peak frequencies are controlled by the source-receiver distance, with higher (lower) peak frequencies indicating shorter (longer) distances between flow front and seismometer. By analysing peak frequencies at different time steps, Lai et al. (2018) propose that one can estimate location and velocity of the flow (Lai et al., 2018). Kean et al. (2015) used their adapted model to invert for sediment cover, and to estimate entrainment rates that compare well with observations.

Here, we study the high frequency content of seismic signals recorded at the debris-flow prone Illgraben torrent, located in Switzerland. This torrent is one of the most active catchments in the Alps (Hürlimann et al., 2003), producing several debris flows per year. In 2017 and 2018, we recorded a total of seven debris flows of different volumes, flow velocities and material composition. We relate spectral characteristics of the debris-flow seismograms to flow-receiver distances, and to topographic features within the torrent. The results show that the spectrum (1) cannot be analyzed as a whole, but has to be segmented in time in order to elucidate characteristics of the debris flow and (2) has to be treated independently for each sensor since the latter are sensitive to different stages of the debris flow.

2. Study site

The Illgraben catchment, located in the southwest of Switzerland, spans from its highest point, the Illhorn (2716 m asl), down to the Rhône Valley where its main torrent, the Illbach, flows into the Rhône River (610 m asl). Past activity within the 9.5 km2 catchment and 5 km long torrent produced a large fan with a radius of about 2 km and a volume of about 500 x 106 m3 (Hürlimann et al., 2003; McArdell et al., 2007). Illgraben is characterized by a complex geology, with the northwest Illhorn face and the head of the trunk channel being dominated by highly fractured quartzite, and the southeast facing slope of the catchment mostly consisting of limestone (Schlunegger et al., 2009; Bennett et al., 2012). The fractured quartzite with erosion rates of tens of centimeters per year is the main contributor to the sediment transported via debris flows (Bennett et al., 2012). Precipitation patterns during summer are characterized by storms, with rainfall intensities of up to several tens of mm/h, and a duration of half an hour to one hour (Hürlimann et al., 2003). In such events, sediment deposited at the head of the trunk channel is mobilized by water gathered along the steep (> 40 degrees) slopes (McArdell et al., 2007). This produces on average 3–5 debris flows per year that contribute significantly to the sediment discharge of the Rhône River (Schlunegger et al., 2009). Typical events have volumes around 20,000 m3 and velocities 3–4 m/s, and transport blocks up to several meters in diameter. In contrast, some events have lower concentration of sediment and fewer such large particles and are more appropriately classified as "debris floods" (e.g. Pierson & Costa, 1987). After a large (3 x 106 m3) rock avalanche in 1961 in the upper catchment, a 48 m tall check dam (CD1, Figure 1) was built within the channel to stabilize the deposit and to prevent large debris

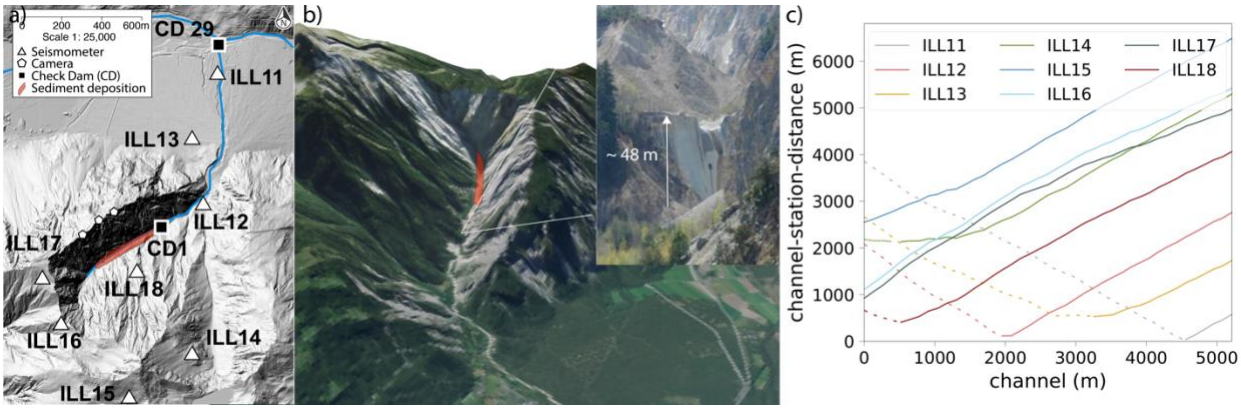

Fig. 1. (a) Overview of the Illgraben catchment and the instrumentation installed during the debris-flow season (June-August) 2018. Seismometer locations (white triangles), the area of sediment supply for the debris flows (shaded red area), and the position of the 48 m tall check dam 1, and check dam 29 (black squares) are depicted (b) 3D orthophoto with sediment deposition area in red and check dam 1 shown on a photo. (c) Channel-receiver distances for all seismic stations installed in 2018. The y-axis represents the distance whereas the x-axis marks the position along the channel (origin at the head of the catchment; 5000m corresponds to the Illbach inflow into the Rhône river). Dashed (continuous) lines show the section where the flow is approaching (moving away from) the station.

flows (Hürlimann et al., 2003). Further downstream along the torrent, 29 additional check dams of several meters height were built to minimize vertical and lateral erosion, thereby stabilizing the channel at the present location. With these measures, most debris flows no longer leave the channel, and damage to infrastructure is rare. To our knowledge, the Illgraben carries little or no discharge in the summer between debris flows, and therefore considerable recreational activity takes place near and in the channel. For this reason, an early warning system was installed in 2000. It is maintained by the Swiss Federal Institute for Forest, Snow and Landscape research (WSL) and consists of radar flow-depth sensors and geophone sensors to provide automatic detection of flows. Upon detection, acoustic alarms are activated and information is sent to local authorities. The data from the early warning system compliments the existing scientific observation station (no warnings are generated) which consists of radar, laser and ultrasonic flow stage sensors at selected check dams, geophones mounted on the downstream facing wall of check dams, as well as video cameras and a 2m x 4m force plate (McArdell et al., 2007; Badoux et al., 2009). Recently, geophone and infrasound sensors have additionally been installed on the fan to increase early warning capabilities (Schimmel et al., 2018; Marchetti et al., 2019). An additional seismic network was installed throughout the Illgraben catchment between May and September in both 2017 and 2018 (Figure 1). This network recorded seven debris flows, and consisted of eight stations with real-time data transfer via the mobile phone network. The interstation distance of the network is about 1.5 km, with an aperture of 5.5 km. Most stations operate with a Lennartz-1s sensor that has a flat response between 1-100 Hz and a sampling rate of 100 Hz. Station ILL11 is equipped with a Trillium compact sensor with a low-frequency corner at 120 seconds.

3. Data: Debris-flow seismograms

During the monitoring period in 2017, three large (> 25,000 m^3) debris flows occurred, with one flow of ~100,000 m3 (Table 1). In 2018 four events were recorded. After the destruction of the force plate in July 2016, volume and flow depth are estimated at the instrumented wall, CD 29 (Figure 1), situated about 10 m upstream of the location of the force plate (Berger et al., 2011). Due to the irregularity of the cross-section shape and the variability in the direction of the approaching flow at this location, flow depths tend to be over-estimated when compared to values previously reported at the force plate. Flow velocity is calculated from the travel time between in-torrent sensors along the channel as described in Schlunegger et al. (2009). As discussed in Section 5, video footage and power spectral densities of the signals suggest a relatively large water content without a boulder-rich front for the first two events in 2018.

Figure 2a shows the seismogram of a debris flow recorded on August 8, 2018. The signal shows the emergent onset and dominant frequencies above 5 Hz, typical for mass movements. The signal emerges from the background noise at a time that depends on the distance between the debris-flow front and the recording station (Walter et al., 2017). For the shown event, amplitudes at different stations vary between 1.5 x 10-3 ms^{-1} at station ILL11, and 2 x 10^{-6} ms^{-1} at

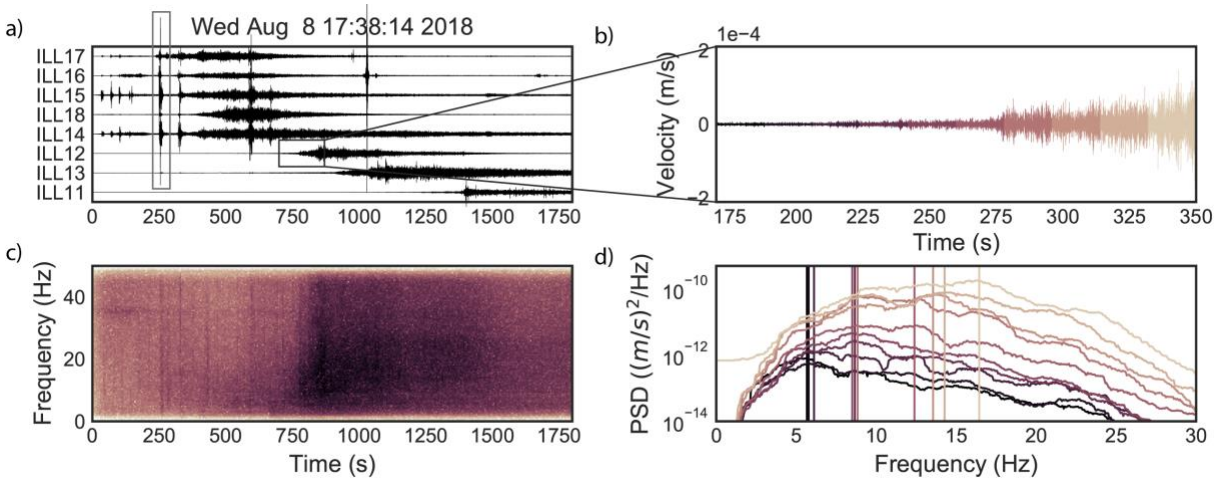

Fig. 2. (a) Seismogram of August 8, 2018 debris flow recorded on all stations of the network. Amplitudes were normalized for each station. Impulsive signals (grey rectangle) are of atmospheric origin (thunderstorm). (b) Close up of onset of the debris-flow signal on station ILL12. Note the emergent onset over several tens of seconds. (c) Spectrogram of signal recorded at station ILL12. The colors show the energy of the frequencies at each time step in decibel, where darker colors represent a higher energy. (d) Spectra of ten time-windows of 18 seconds corresponding to the color-coded waveform in (b). The spectra are smoothed with a 1 Hz running average. The vertical lines mark the peak amplitude of the spectral power.

ILL16. High amplitude impulsive signals on some stations within the network are of atmospheric origin, generated by thunder, and not directly related to the debris-flow signal (Marchetti et al., 2019).

Between debris flows, seismic background noise at Illgraben is dominated by several almost discrete frequency bands (Fig. 3). Between 1 and 5 Hz, anthropogenic noise is present showing diurnal variation, as well as lower energy on both weekends and public holidays compared to work days. Though strong, this signal is unlikely to affect seismic detectability of debris flows (Walter et al., 2017). Another distinct frequency band of noise is found at about 15 Hz. Within this band, an abrupt decrease in power can be observed at the end of June of both 2017 and 2018. We suggest that this could either be related to water discharge in the catchment due to snow melt, or to a change in hydropower operations at a dam 3 km away from the seismic station.

Here we concentrate on the frequency spectrum of the signal directly before and during the debris-flow events. We focus on station ILL12, because its near-torrent location implies a large range of distances to the flow front, both up and down-stream (Figure 1c). Such distance variations are particularly important for investigating variations in frequency signature (Lai et al., 2018). The goal is, to separate source and path effects on the frequency content of the signal, to constrain source mechanisms.

4. Peak frequency migration

For all 2017 and 2018 debris flows we computed the frequency spectrum for signal bins of 5 s with an overlap of 2.5 s. Figure 2c shows a close up of the initiation of the debris flow on August 8, 2018, with Figure 2d showing the corresponding color-coded spectra. As expected, the spectra show a peak migration from about 5.5 Hz towards higher frequencies for the flow front approaching station ILL12.

Table 1 Characteristics of the seven debris flows recorded in 2017 and 2018 (n.a. denotes that estimates are not yet available for 2018). “CD1” stands for “check dam 1”.

Date	Arrival time CD1 (UTC)	Volume (m^3)	Velocity (m/s)	Flow depth (m)
2017-05-29	16:58:31	100000	6.7	4.8
2017-06-03	23:27:38	25000	5.1	3.3
2017-06-14	19:30:48	35000	7.1	3.4
2018-06-11	10:46:39	35000	7.0	3.5
2018-06-12	18:29:16	n.a.	n.a.	n.a.
2018-07-25	16:56:40	< 50000	4.69	2.0
2018-08-08	17:49:25	< 100000	6.70	n.a.

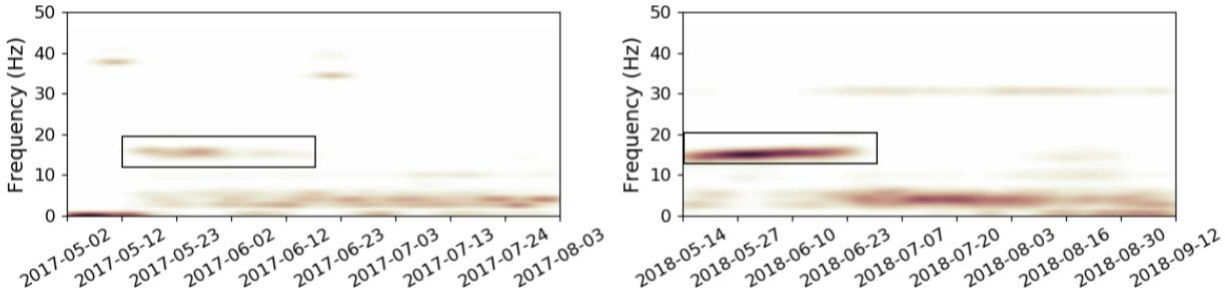

Fig. 3. Density plot of peak frequencies at station ILL12 for both 2017 and 2018. The rectangles mark a discrete noise band at about 15 Hz. The noise-source stops in June for both years. We suggest this to be either related to snow melt or to a change in nearby hydropower operations.

Figure 4a shows the peak frequencies at each time step for all recorded events. As a result of the broadband nature of the debris-flow seismograms, peak frequencies are difficult to identify in conventional spectrograms (Figure 2b). Only peak frequencies corresponding to a spectral power above 1 x 10^{-13} ms^{-2} Hz^{-1} were plotted, to eliminate low energy background noise caused by anthropogenic and discharge-related seismicity. In-torrent geophone-counts at CD1 of the August 8, 2018 event are shown additionally. The geophones, which measure the vertical velocity of ground vibration, start recording when the front of the debris flow reaches the check dam. The signal is represented as impulses that exceed a certain threshold (e.g. McArdell et al., 2007). In Figure 4a, all events were aligned according to the first recording of the geophone impulses, hence the arrival of the flow at CD1. The 48 m drop at CD1 leads to a shift in dominant frequencies from pre-event noise bands of 1-5Hz and 15Hz to about 5.5 Hz for all events and an overall increase in spectral power (Figure 4a, dashed black line). Observations of flow over CD1 are not available, however, given that debris-flow velocities are relatively large, it is likely that the flow is largely detached from the face of the spillway and that it resembles free-fall conditions. Note that with the imposed energy threshold, the two small events of June 2018 do not emerge from the background noise. After the flow fronts pass CD1 and the 48 m free fall, the dominant frequencies rise to around 15 Hz when directly passing the station. After the initial rise, dominant frequencies shift between 12 and 25 Hz, but no time-dependent pattern can be observed (Figure 4a, dotted black line). In contrast to the frequency domain, the signal of the free fall cannot be distinguished from background noise in the time domain as has been observed at other sites (Coviello et al., 2015; Schimmel et al., 2018).

The evolution from low to higher peak frequencies can also be observed at station ILL11 and ILL13 (Appendix A). The stations have a minimum distance to the channel of 30 and 700 m, respectively. ILL18, which is closest to the initiation area of the flow, does not show a clear pattern in dominant frequencies. This can be explained by signal mixing of noise sources that are close to this station (i.e. precipitation and runoff concentration from the slopes, discharge, and 48 m channel step at CD1). For stations farther away from the channel, no pattern in dominant frequencies can be observed either. Specifically, stations that are farther away than 1 km from the channel (ILL14, 15, 16, 17) do not capture the peak frequency migration. For these stations, the 48 m free fall at CD1 may be too far to generate a signal that dominates over other seismic sources at the head of the trunk channel, closer to the stations.

5. Debris-flow characteristics from seismic signals

Next, we investigate the origin of the frequency signature of the flows in order to connect the findings with flow characteristics. The model by Lai et al. (2018), predicts the following power spectral density P as a function of frequency f of the seismic signal generated by the boulder-rich debris-flow front:

$$P \approx 1.9\, LWD^3u^3 \times \frac{f^{3+5\xi}}{v_c^5 r_0} e^{-\frac{8.8 f^{1+\xi} r_0}{v_c Q}} \quad (1)$$

L and W are the debris-flow head length and width, respectively, D is the 94th percentile of the grain size diameter, u is the flow velocity, and r_0 is the average distance between the debris-flow front and the receiver. Equation 1 shows, that the peak frequency is mostly dependent on the distance between source and receiver. The amplitude of the signal, however, linearly scales with the length and the width of the debris-flow front, as well as with the third power of particle size and flow velocity.

Using values of 500±100 m/s for Rayleigh-wave phase velocity v_c, 60±10 for the quality factor Q, and 0.417±0.05 for ξ (Tsai et al., 2012; Burtin et al., 2014; Burtin et al., 2016; Lai et al., 2018), Equation (1) places the sources of the

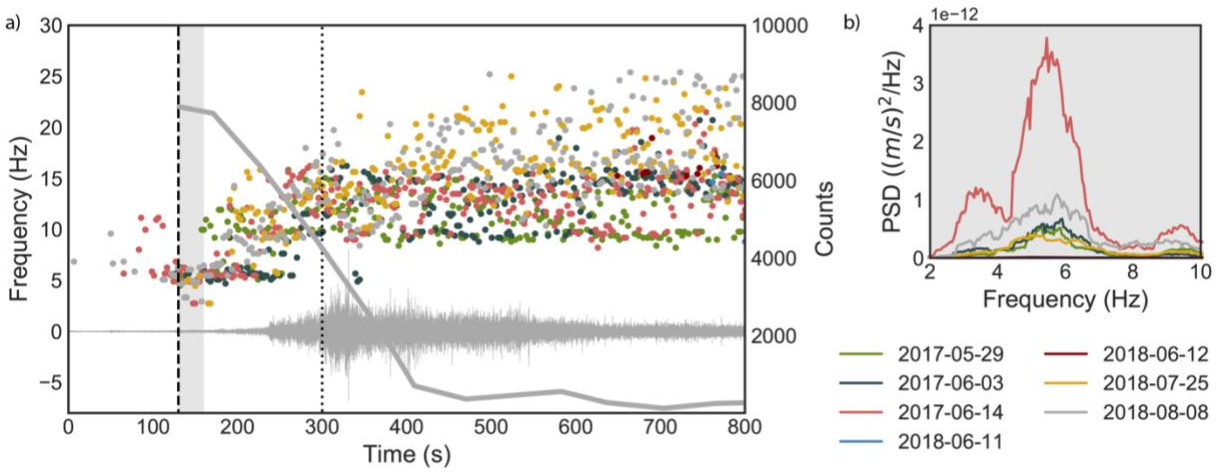

Fig. 4. (a) Peak frequencies for all events in 2017 and 2018, binned for time steps of 2.5 s (dots), together with geophone counts recorded at CD1 for August 8, 2018 event (grey line). The grey signal shows the waveform of the August 8, 2018 event recorded on station ILL12. The events were aligned according to the onset of the geophone measurements at CD1. The peak frequencies are plotted for power spectral densities that exceed 1 x 10^{-13} $(ms^{-1})^2$ Hz^{-1}. The shaded area shows the time span used to calculate the spectra in (b). The dashed line marks the onset of the geophone recordings at CD1 and the corresponding frequency drop to 5.5 Hz. The dotted line marks the approximate passage of the debris flow at ILL12 which corresponds to a change in frequency pattern. Note the increase in dominant frequencies after the passage of CD1 until passing station ILL12. (b) Spectra of all events 30 seconds after passing CD1. The spectra are smoothed with a 1 Hz running average. The June 14, 2017 event clearly shows the highest power spectral density at that time.

two dominant frequency bands of 5.5 Hz and 15 Hz at distances of about 1100±500 m and 300±150 m from ILL12, respectively. This corresponds to the distance between (a) the station and CD1, and (b) the smallest distance between the station and the channel, which lies for both cases within the uncertainties. Due to model simplifications and poorly constrained site effects, the distance is only a rough estimate. Nevertheless, it suggests that the main sources for the seismic waves recorded at ILL12 are the flow over the spillway at CD1 and the processes that happen at small distances from the station. Lai et al. (2018) use the continuous increase in peak frequencies to estimate flow velocity. At Illgraben, the two distinct dominant sources inhibit estimation of flow velocity, as the jump in frequency reflects the time when the dominance of the two signals changes, rather than a location of the flow front.

Next, we compare the different event spectra recorded at Station ILL12 when the flow fronts pass CD1 (Fig. 4b). The spectra are computed over 30s, and a running average of 1 Hz was applied. We assume that at these time intervals, the signals are dominated by seismic waves generated by boulder impacts at the base of the 48 m free fall at CD1. At this moment, projectile motion of the boulders implies that vertical flow (impact) velocities are the same for all events. Length of the front and width are therefore expected to be similar, assuming that the flow front impact lasts longer than the 30 s-long time window used to calculate the spectra. To only concentrate on the 5.5 Hz signals generated at CD1, the signal was filtered between 3 and 10 Hz. According to Equation (1), differences in spectra, in particular spectral amplitudes, are then attributable to grain size differences. The largest amplitude of power spectral density is generated by the event on June 14, 2017. Unfortunately, no video material is available for this event since it happened at night. Therefore, a cross validation to check whether the largest power is generated by larger boulder size in the debris-flow front, is not possible. When comparing the debris flow on May 29, 2017 with other events, one can observe that the energies are similar to the events on July 25 and August 8 in 2018. The videos indicate the presence of large boulders in all three flows, but a quantitative statement on the 94th percentile of the particle sizes is difficult. The small events in June 2018 show the lowest spectral energies, which suggests that particle sizes for these flows are substantially smaller than for other events. Analysis of the videos for the 2018 events has not yet been completed, but preliminary analysis suggests that these events might be debris floods rather than debris flows.

6. Conclusion

The source mechanism of seismic signals of debris flows is strongly dependent on particle sizes and topographic features of the flow path. Seismic studies of debris-flow dynamics and material composition should therefore not focus on the entire (temporally averaged) debris-flow seismograms, but on individual time windows. The spectral content of the signal can be dominated by large topographical features, such as the free fall behind a check dam in our case.

Fig. 5. Pictures of five debris flows at check dam 29 at the lowermost part of the torrent. Pictures of the events of June 3 and June 14, 2017 do not give any insight on particle sizes, as they happened during night time. The pictures in the first row show the large event on May 29, 2017 (left), and the event on August 8, 2017 (right) that has been used as an example in Fig. 2.

Large uncertainties of the seismic properties of the torrent catchment's sub-surface inhibit accurate models of the seismic propagation between flow front and recording unit. This complicates the interpretation of seismograms in terms of flow properties.

Acknowledgements

The project is funded by WSL's strategic initiative Climate Change Impacts on Alpine Mass Movements (CCAMM). FW's salary was funded by the Swiss National Science Foundation (GlaHMSeis Project PP00P2_157551). The municipally of Leuk and Anniviers generously provided permission and assistance for the seismometer deployment. We thank the Swiss Seismological Service who supported the project with seismic stations, real time data transfer and archiving facilities as well as manpower in the field. Alexandre Badoux and Christoph Graf assisted in the field campaign planning. We also thank the VAW and WSL personal, especially Martin Funk, for technical and scientific input and support in the field. The authors are grateful to Kate Allstadt and Velio Coviello for detailed and constructive reviews.

Online content

The data and code that was used in this study are available in the deciphering_debris-flow_seismograms git repository, https://github.com/michaelawenner/deciphering_debris-flow_seismograms

References

Allstadt, K. E., Matoza, R. S., Lockhart, A., Moran, S. C., Caplan-Auerbach, J., Haney, M., ... & Malone, S. D., 2018, Seismic and acoustic signatures of surficial mass movements at volcanoes: Journal of Volcanology and Geothermal Research,v. 364, p. 76-106.

Arattano, M., & Marchi, L., 2008, Systems and sensors for debris-flow monitoring and warning: Sensors, v. 8(4), p. 2436-2452.

Badoux, A., Graf, C., Rhyner, J., Kuntner, R., & McArdell, B. W., 2009, A debris-flow alarm system for the Alpine Illgraben catchment: design and performance: Natural hazards, v. 49(3), p. 517-539.

Bennett, G. L., Molnar, P., Eisenbeiss, H., & McArdell, B. W., 2012, Erosional power in the Swiss Alps: characterization of slope failure in the Illgraben: Earth Surface Processes and Landforms, v. 37(15), p. 1627-1640.

Berger, C., McArdell, B. W., & Schlunegger, F., 2011, Direct measurement of channel erosion by debris flows, Illgraben, Switzerland: Journal of Geophysical Research: Earth Surface, v. 116(F1).

Burtin, A., Bollinger, L., Vergne, J., Cattin, R., & Nábělek, J. L., 2008, Spectral analysis of seismic noise induced by rivers: A new tool to monitor spatiotemporal changes in stream hydrodynamics. Journal of Geophysical Research: Solid Earth, v. 113(B05301).

Burtin, A., Hovius, N., McArdell, B. W., Turowski, J. M., & Vergne, J., 2014, Seismic constraints on dynamic links between geomorphic processes and routing of sediment in a steep mountain catchment: Earth Surface Dynamics, v. 2(1), p. 21-33.

Burtin, A., Hovius, N., & Turowski, J. M.,2016, Seismic monitoring of torrential and fluvial processes: Earth Surface Dynamics, v. 4(2), p. 285-307.

Christen, M., Kowalski, J., & Bartelt, P., 2010, RAMMS: Numerical simulation of dense snow avalanches in three-dimensional terrain: Cold Regions Science and Technology, v. 63(1-2), p. 1-14.

Coviello, V., Arattano, M. and Turconi, L., 2015, Detecting torrential processes from a distance with a seismic monitoring network: Natural Hazards, v. 78(3), p. 2055-2080.

Dammeier, F., Moore, J. R., Haslinger, F., & Loew, S., 2011, Characterization of alpine rockslides using statistical analysis of seismic signals: Journal of Geophysical Research, Earth Surface, v. 116(F4), p. 1-19.
Deparis, J., Jongmans, D., Cotton, F., Baillet, L., Thouvenot, F., & Hantz, D., 2008, Analysis of rock-fall and rock-fall avalanche seismograms in the French Alps: Bulletin of the Seismological Society of America, v. 98(4), p. 1781-1796.
Dietze, M., Turowski, J. M., Cook, K. L., & Hovius, N., 2017, Spatiotemporal patterns, triggers and anatomies of seismically detected rockfalls: Earth Surface Dynamics, v. 5(4), p. 757.
Ekström, G., & Stark, C. P., 2013, Simple scaling of catastrophic landslide dynamics: Science, v. 339(6126), p. 1416-1419.
Heck, M., Hammer, C., Herwijnen, A. V., Schweizer, J., & Fäh, D., 2018, Automatic detection of snow avalanches in continuous seismic data using hidden Markov models: Natural Hazards and Earth System Sciences, v. 18(1), p. 383-396.
Hibert, C., Mangeney, A., Grandjean, G., & Shapiro, N. M., 2011, Slope instabilities in Dolomieu crater, Réunion Island: From seismic signals to rockfall characteristics: Journal of Geophysical Research, Earth Surface, v. 116(F4), p. 1-18.
Hibert, C., Mangeney, A., Grandjean, G., Peltier, A., DiMuro, A., Shapiro, N. M., ... & Kowalski, P.,2017, Spatio-temporal evolution of rockfall activity from 2007 to 2011 at the Piton de la Fournaise volcano inferred from seismic data: Journal of Volcanology and Geothermal Research, v. 333, p. 36-52.
Hürlimann, M., Rickenmann, D., & Graf, C., 2003, Field and monitoring data of debris-flow events in the Swiss Alps: Canadian geotechnical journal, v. 40(1), p. 161-175.
Kean, J. W., Coe, J. A., Coviello, V., Smith, J. B., McCoy, S. W., & Arattano, M., 2015, Estimating rates of debris flow entrainment from ground vibrations: Geophysical Research Letters, v. 42(15), p. 6365-6372.
Lai, V. H., Tsai, V. C., Lamb, M. P., Ulizio, T. P., & Beer, A. R., 2018, The Seismic Signature of Debris Flows: Flow Mechanics and Early Warning at Montecito, California: Geophysical Research Letters, v. 45(11), p. 5528-5535, doi: 10.1029/2018GL077683.
Larose, E., Carrière, S., Voisin, C., Bottelin, P., Baillet, L., Guéguen, P., ... & Gimbert, F., 2015, Environmental seismology: What can we learn on earth surface processes with ambient noise?: Journal of Applied Geophysics, v. 116, p. 62-74.
Mangeney-Castelnau, A., Bouchut, F., Vilotte, J. P., Lajeunesse, E., Aubertin, A., & Pirulli, M., 2005, On the use of Saint Venant equations to simulate the spreading of a granular mass: Journal of Geophysical Research, Solid Earth, v. 110(B9).
Mangeney, A., Tsimring, L. S., Volfson, D., Aranson, I. S., & Bouchut, F. (2007). Avalanche mobility induced by the presence of an erodible bed and associated entrainment. Geophysical Research Letters, 34(22),doi: 10.1029/2007GL031348.
Marchetti, E., Walter, F., Barfucci, G., Genco, R., Wenner, M., Ripepe, M., et al., 2019. Infrasound array analysis of debris flow activity and implication for early warning: Journal of Geophysical Research: Earth Surface, v. 124, doi: 10.1029/2018JF004785.
McArdell, B. W., Bartelt, P., & Kowalski, J., 2007, Field observations of basal forces and fluid pore pressure in a debris flow: Geophysical Research Letters, v. 34(7), doi: 10.1029/2006GL029183.
Norris, R. D., 1994, Seismicity of rockfalls and avalanches at three Cascade Range volcanoes: Implications for seismic detection of hazardous mass movements: Bulletin of the Seismological Society of America, v. 84(6), p. 1925-1939.
Pierson, T. C., & Costa, J. E., 1987, A rheologic classification of subaerial sediment-water flows. Debris flows/avalanches: process, recognition, and mitigation: Reviews in Engineering Geology, v. 7, p. 1-12.
Provost, F., Hibert, C., & Malet, J. P., 2017, Automatic classification of endogenous landslide seismicity using the Random Forest supervised classifier: Geophysical Research Letters, v. 44(1), p. 113-120.
Schimmel, A., Hübl, J., McArdell, B. W., & Walter, F., 2018, Automatic Identification of Alpine Mass Movements by a Combination of Seismic and Infrasound Sensors: Sensors, v. 18(5), p. 1658.
Schlunegger, F., Badoux, A., McArdell, B. W., Gwerder, C., Schnydrig, D., Rieke-Zapp, D., & Molnar, P., 2009, Limits of sediment transfer in an alpine debris-flow catchment, Illgraben, Switzerland: Quaternary Science Reviews, v. 28(11-12), p. 1097-1105.
Suriñach, E., Vilajosana, I., Khazaradze, G., Biescas, B., Furdada, G., & Vilaplana, J. M., 2005, Seismic detection and characterization of landslides and other mass movements: Natural Hazards and Earth System Science, v. 5(6), p. 791-798.
Tsai, V. C., Minchew, B., Lamb, M. P., & Ampuero, J. P., 2012, A physical model for seismic noise generation from sediment transport in rivers: Geophysical Research Letters, v. 39(2), doi: 10.1029/2011GL050255.
Vilajosana, I., Surinach, E., Abellán, A., Khazaradze, G., Garcia, D., & Llosa, J., 2008, Rockfall induced seismic signals: case study in Montserrat, Catalonia: Natural Hazards and Earth System Sciences, v. 8(4), p. 805-812.
Walter, F., Burtin, A., McArdell, B. W., Hovius, N., Weder, B., & Turowski, J. M., 2017, Testing seismic amplitude source location for fast debris-flow detection at Illgraben, Switzerland: Natural Hazards and Earth System Sciences, v. 17(6), p. 939-955.

Appendix A. Signals at other seismic stations

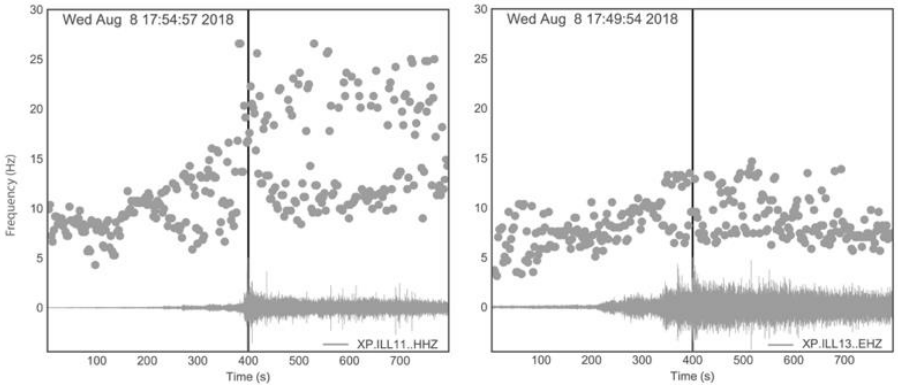

Fig. A1. Seismic signal and corresponding dominant frequencies of the August 8, 2018 event recorded at stations ILL11 and ILL13.